

A symbolically defined InP double heterojunction bipolar transistor large-signal model

Cao Yuxiong(曹玉雄), Jin Zhi(金智)[†], Ge Ji(葛霁), Su Yongbo(苏永波), and Liu Xinyu(刘新宇)

(Institute of Microelectronics, Chinese Academy of Sciences, Beijing 100029, China)

Abstract: A self-built accurate and flexible large-signal model based on an analysis of the characteristics of InP double heterojunction bipolar transistors (DHBTs) is implemented as a seven-port symbolically defined device (SDD) in Agilent ADS. The model accounts for most physical phenomena including the self-heating effect, Kirk effect, soft knee effect, base collector capacitance and collector transit time. The validity and the accuracy of the large-signal model are assessed by comparing the simulation with the measurement of DC, multi-bias small signal S parameters for InP DHBTs.

Key words: InP DHBT; large-signal model; SDD

DOI: 10.1088/1674-4926/30/12/124006

EEACC: 1220; 6185; 9240C

1. Introduction

Heterojunction bipolar transistors (HBTs) have become very promising devices for different applications at microwave and millimeter wave frequencies. Due to velocity modulation and the current blocking effect, the Si-bipolar transistor model is not sufficient to model 305 GHz^[1] (f_{\max}) InP/InGaAs double heterojunction bipolar transistors (DHBTs). Thus, in the design of high performance microwave circuits, an accurate device model valid for a wide range of bias and signal frequencies is imperative.

The GP^[2] and VBIC^[3] models were developed for BJT physics, where the base transit time dominated, which was not the case with HBTs. The HICUM^[4] and MEXTRAM^[5] models were based on Si/SiGe HBTs, where the velocity modulation is different from GaAs and InP HBTs. Higher electron velocities occur at low field for GaAs and InP HBTs, and the highest f_t tends to occur at low V_{ce} levels. The UCSD^[6] and FBH^[7] models were mainly based on GaAs-based HBTs, which have some different characteristics to InP-based DHBTs. In addition, the InP HBT process is developing and can introduce some new effects. Therefore these models should be modified to fit the InP HBT physics. A self-built InP HBT model which can be conveniently modified is imperative for the continuously developing technology. Reference [8] has presented a new modified VBIC model and obtained a more accurate fitting between the measurement and the simulation below the Kirk current, but some new effects are hard to add to the model and can possibly introduce convergence problems.

The purpose of the paper is to set up a self-built flexible nonlinear large-signal InP HBT model, which is implemented as a symbolically defined device (SDD)^[9] in an Agilent ADS simulator. The large-signal model includes most characteristics of InP HBTs. The self-heating effect^[3] is expressed by an RC thermal sub-circuit. The soft knee effect^[10] which results

from the potential spike in InP DHBT is modeled by a bias-dependent collector resistance. The usage of τ_{kirk} defines the extra increased delay time caused by high collector current^[11]. Due to improving technology, some new effects occurring in the device can be conveniently added into the SDD. The validity of the model is demonstrated by comparing the DC, multi-bias S parameters simulations to measurements up to 26.1 GHz for a $1 \times 15 \mu\text{m}^2$ emitter-area InGaAs/InP DHBT.

2. HBT model

2.1. Model topology

The improved HBT model is based on the Gummel-Poon integral charge-control relation and incorporates many physical mechanisms, including self-heating, DC current blocking, velocity modulation, Kirk effect and peripheral parasitic. Figure 1 shows the equivalent circuit diagram of the adopted large-signal model topology without the pad parasitic part. The intrinsic model is bounded by the dashed box.

2.2. DC current model

The DC equations are based on the VBIC model. The base-emitter current and the base-collector current covers the ideal and non-ideal (recombination) behavior.

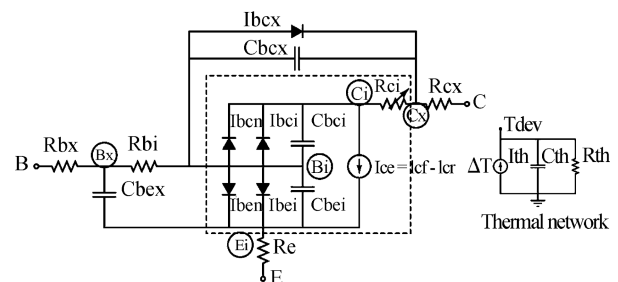


Fig. 1. Large-signal equivalent circuit diagram for modeling InP DHBTs.

[†] Corresponding author. Email: jinzhi@ime.ac.cn

Received 5 June 2009, revised manuscript received 13 July 2009

$$I_{bx} = I_{bxn} + I_{bxi} = IBXN \times \left(\exp \frac{V_{bxi}}{n_{XN} v_t} - 1 \right) + IBXI \times \left(\exp \frac{V_{bxi}}{n_{XI} v_t} - 1 \right). \quad (1)$$

Two parallel diode currents are used: one for the ‘ideal’ part (index I) and the other for the ‘non-ideal’ part (index N) of the base–collector or base–emitter current. The variable x in the formula is used to denote either base–collector (C) or base–emitter (E). IBXN and IBXI are the non-ideal and ideal saturation current, respectively. n_{XN} and n_{XI} are the non-ideal and ideal current ideality factor, respectively. V_{bxi} is the junction voltage and v_t is the temperature voltage.

The diode current I_{bcx} is the extrinsic part of the base–collector current.

The collector current source I_{ce} is determined by the two transport current terms I_{cf} and I_{cr} :

$$I_{ce} = I_{cf} - I_{cr} = I_s \left(\exp \frac{V_{beci}}{n_f v_t} - 1 \right) - I_{sr} \left(\exp \frac{V_{beci}}{n_r v_t} - 1 \right), \quad (2)$$

where I_s and n_f are the forward collector saturation current and ideality factor, respectively. I_{sr} and n_r are the reverse emitter saturation current and ideality factor, respectively.

For InP DHBTs, the presence of conduction band spikes at PN junctions can result in additional transport mechanisms such as thermionic emission over the barrier and tunneling through it. A spike at a wide-bandgap collector can also block carriers exiting the base, causing increased recombination, lower beta, and the ‘soft knee’ effect, where the device enters saturation at a higher collector voltage^[10]. The I_c – V_{ce} curves of the DHBT device show a knee round-off, especially at high current density. The effect is implemented by an increase in collector resistance with the collector current^[12]:

$$R_{ci} = a I_c^b \times \tanh \left(\frac{I_c}{I_0} \right), \quad (3)$$

where a , b , I_0 are the fitting parameters.

2.3. AC model

High-frequency performance is defined by charge model; therefore, the AC characteristic includes depletion charge and diffusion charge. The depletion charge for both the base–emitter and base–collector junctions is based on the formulation from the HICUM model^[10]. The model equation defines three regions of forward bias, low reverse bias and high reverse bias with a conventional capacitance formula and limiting function. This formulation and its derivatives are fully continuous for all regions of bias and therefore appropriate for a large-signal HBT model. Detailed methods are given in Ref. [4].

The diffusion charge of the model has a direct impact on the delay, especially the collector delay charge, since its complex bias dependence has several important consequences for the performance of the device. This model adopts Masaya Iwamoto’s collector transit time equations^[13]. The transit time $\tau(V_{bc}, I_c)$ is current and voltage dependent, and consists of

three components: base transit time (τ_b), excess delay due to Kirk effect (τ_{kirk}), and collector transit time (τ_c).

$$\tau(V_{bc}, I_c) = \tau_b + \tau_{kirk} + \tau_c. \quad (4)$$

The base transit time (τ_b) is assumed to be constant due to the heavily doped metallurgical base. A reasonable approximation can be made and the charge is simple^[13]:

$$Q_{tb} = \tau_b I_{cf}. \quad (5)$$

Current blocking and velocity modulation can affect the HBT high-frequency performance. Therefore, τ_{kirk} accounts for the delay due to the Kirk effect at high current injection and is also borrowed from the HICUM model^[4].

$$Q_{kirk} = \tau_{kirk} I_{cf} \exp(V_{bc}/VKRK + I_{cf}/IKRK). \quad (6)$$

IKRK is the critical current for the Kirk effect, and VKRK is the change of IKRK with V_{bc} . The Kirk charge should generally account for the increase in transit time at high currents; for example, the f_i roll-off in DHBTs.

The collector transit time mainly accounts for the electric field dependence of the electron velocity. Due to the negative differential mobility characteristics of InP, it is possible to obtain higher electron velocities at lower voltages compared to the saturated velocity at high voltages. τ_c is also current dependent since electrons compensate the positive ionized impurity charges in the collector depletion region. The collector transit time can be approximated with $0.5(1+\tanh)$ as a function of I_{cf} given by^[13],

$$\tau_c = \text{PTCMIN} \left(1 - \frac{V_{bc,eff}}{VTCMIN} \right) + \frac{1}{2} \text{TFC0} \left(1 - \frac{V_{bc,eff}}{VTC0} \right) \times \left[1 + \tanh \frac{\text{ITC} \left(1 - \frac{V_{bci}}{VTC} \right) - I_{cf}}{\text{ITC2} \left(1 - \frac{V_{bci}}{VTC2} \right)} \right], \quad (7)$$

$$V_{bc,eff} = \text{VKTR} \ln \left(\exp \frac{\text{VKMX} + V_{bci}}{\text{VKTR}} + 1 \right) - \text{VKMX}, \quad (8)$$

where $V_{bc,eff}$ models the nonlinear dependence of electron velocity with voltage, TFC0 is low current transit time, TCMIN is high current transit time, ITC is the midpoint in the collector current between TFC0 and TCMIN, ITC2 is the width in the collector current between TFC0 and TCMIN, VTC0 is the change of TFC0 with V_{cb} , VTC is the change of ITC with V_{cb} , VTC2 is the change of ITC2 with V_{cb} , VKMX is the maximum V_{cb} , and VKTR is the transition width in V_{cb} to VKMX.

2.4. Thermal network

When I_c increases, the junction temperature increases, which in turn lowers the value of the electron saturation velocity. This is the increasing back-injection current with temperature, which causes the current gain to fall off. The phenomenon can be observed from Fig. 4. When V_{ce} increases, I_c decreases in the high current and high voltage region.

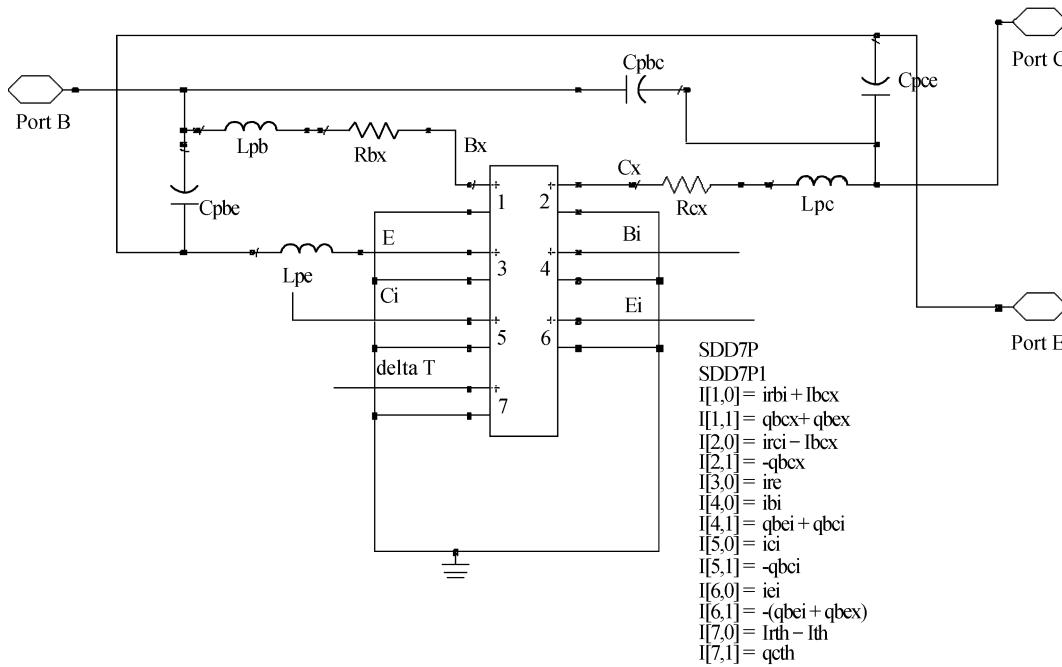


Fig. 2. Complete large-signal InP DHBT model.

The self-heating is defined by the thermal RC network on the right of Fig. 1. The transistor's instantaneous dissipated power is used as the source for the thermal network. The RC network source and the temperature constitute a positive feedback. The phenomena can be expressed by the simulator to iterate a self-consistent solution. The equation is given as:

$$P_{diss} = \frac{\Delta T}{R_{th}} + C_{th} \frac{d\Delta T}{dt}. \quad (9)$$

where $\Delta T = T_{dev} - T_{nom}$, T_{dev} is the transistor internal temperature and T_{nom} is the room temperature. C_{th} and R_{th} are the thermal capacitance and resistance, respectively.

3. Model implementation

The model will be implemented with a complete SDD model in Agilent ADS. These components are multi-port devices that can be modeled directly on a schematic. An SDD can be defined by specifying equations that relate port currents, port voltages, and their derivatives^[9]. It is convenient to add and modify various effects in the SDD. The SDD offers a simple, fast way to develop and modify complex models.

The SDD model is equivalent to the large-signal model with pad parasitic and is illustrated in Fig. 2. The nodes of the model topology in Fig. 1 correspond to the ports of SDD in Fig. 2. It can directly use the SDD model for a circuit simulation and change the model by modifying the equations in the variables and equations component.

The capacitances and inductors outside the SDD component in Fig. 2, such as C_{pce} , C_{pbe} , C_{pbc} , L_{pb} , L_{pc} , and L_{pe} , are the parasitic part, and are decided by pads. R_{bx} , R_{cx} , and R_e integrated in the SDD are the access resistances. The intrinsic capacitances C_{bei} , C_{bci} and extrinsic capacitances C_{bex} , C_{bcx} in

the model are indicated by the derivation of q_{bei} , q_{bci} , q_{bex} , and q_{bcx} , respectively.

The large-signal model includes DC and AC parts, so each port consists of two parts. Port two (the extrinsic collector node Cx) consists of the DC current: the current of resistance r_{ci} (i_{rci}) and the diode current I_{bcx} and the AC current: the current of capacitances C_{bcx} . The definition of the other ports is analogous with port one except port seven. Due to the self-heating iterating being self-consistent, we define port seven as an iterated variable ΔT . ΔT increases with P_{diss} , and vice versa. The related equations are defined in the variables and equations component.

4. Model verification and discussion

The parameter extraction procedure starts from de-embedding the parasitic parameters, then extracts the access resistances using fly-back measurements but the resistances are retuned to fit S -parameters at cold-HBT conditions. The small-signal intrinsic equivalent circuit parameters are extracted using direct techniques without the optimization reported previously^[14, 15]. The large-signal intrinsic circuit parameters have been extracted from a large number of small-signal S -parameters with multi-bias points.

A $1 \times 15 \mu m^2$ emitter-area InGaAs/InP DHBT device is used to validate the proposed model. The forward and reverse Gummel plots are shown in Fig. 3. Figure 4 shows the $I_c - V_{ce}$ curve comparison between the measurement and simulation.

In addition to the output DC $I-V$ and Gummel characteristics, the model is validated by comparing the measured and simulated S -parameters over a bias range of collector current from 1 to 16 mA and across a frequency range of 0.1 to 26.1 GHz. Figures 5 and 6 show the fitting of S -parameters for

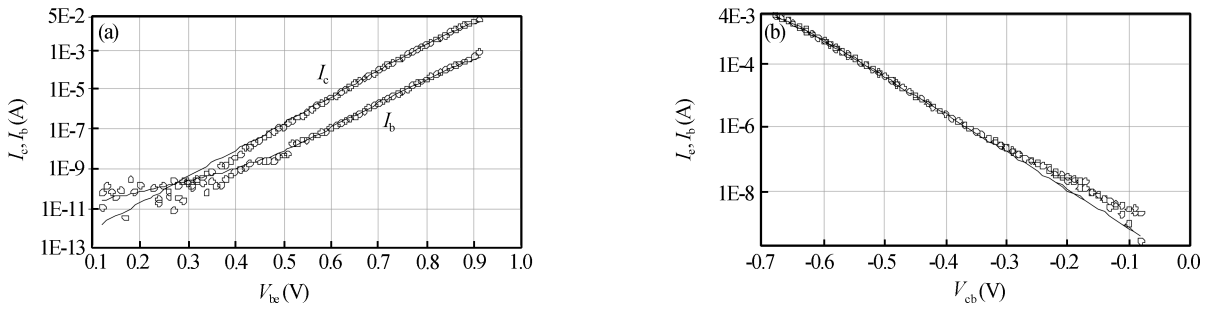


Fig. 3. Modeled (solid) versus measured (symbol-dot): (a) Forward Gummel plot; (b) Reverse Gummel plot.

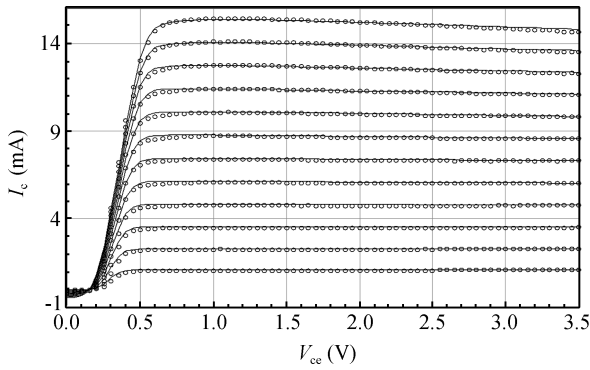


Fig. 4. Modeled (solid) versus measured (symbol-dot) I_c - V_{ce} . I_b is from 20 to 240 μ A in steps of 20 μ A.

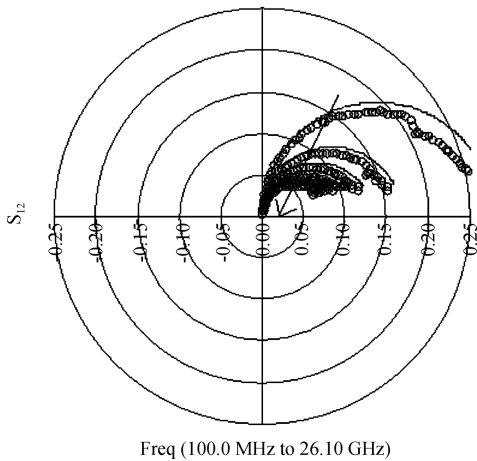
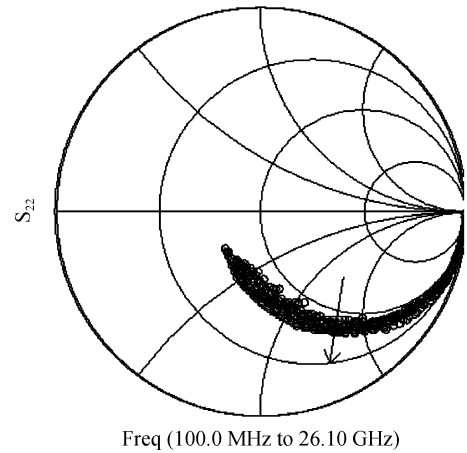
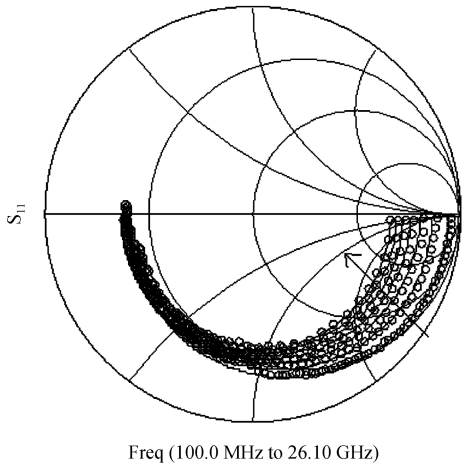
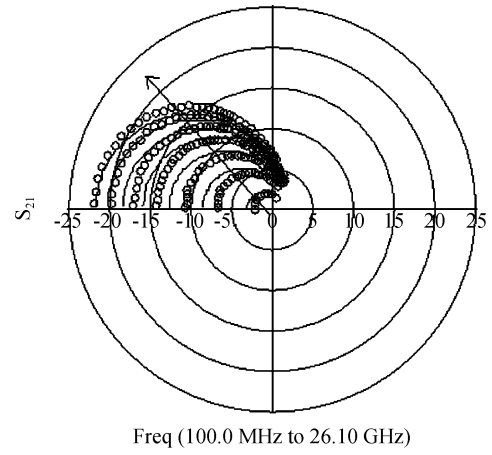


Fig. 6. Modeled (solid) versus measured (symbol-dot): S_{21} , S_{22} for $I_c = 1$ to 16 mA and $V_{ce} = 2$ V. The arrow direction indicates increasing I_c .

Fig. 5. Modeled (solid) versus measured (symbol-dot): S_{11} , S_{12} for $I_c = 1$ to 16 mA and $V_{ce} = 2$ V. The arrow direction indicates increasing I_c .

$V_{ce} = 2$ V and I_c varying from 1 to 16 mA, corresponding to current densities of 0.07–1.07 mA/ μ m².

There is some deviation in the model versus measured data in the low current and low frequency region in S_{21} . The model formulation is done on a certain region for a special application. In this paper, the main interest is in the operation region ($I_c = 10$ mA), and it is seen to show better fitting in this region.

5. Conclusions

A nonlinear circuit simulation model for InP DHBTs based on charge formulation and an accurate large-signal model is implemented by using a seven port SDD in Agi-

lent ADS. The model is flexible to modification due to the equation-based SDD component. This model accounts for the self-heating effect, Kirk effect, base collector capacitance and collector transit time bias dependence. The model is assessed by comparing its simulation results to measurements: DC, multi-bias S -parameters for a $1 \times 15 \mu\text{m}^2$ emitter area InGaAs/InP DHBT. The obtained results show that the presented model and the measurement are in good agreement over a wide bias range.

References

- [1] Jin Z, Su Y, Cheng W, et al. Common-base multi-finger submicron InGaAs/InP double heterojunction bipolar transistor with f_{max} of 305 GHz. *Solid-State Electron*, 2008, 52(11): 1825
- [2] Gummel H K, Poon H C. An integrated charge control model of bipolar transistors. *Bell Syst Tch J*, 1970, 49: 829
- [3] McAndrew C C, Seitchik J A, Bowers D F, et al. VBIC95, the vertical bipolar inter-company model. *IEEE J Solid-State Circuits*, 1996, 31(10): 1476
- [4] http://www.iee.et.tu-dresden.de/iee/eb/comp_mod.html. HICUM HBT model. 2002
- [5] http://www.nxp.com/models/bi_models/mextram/. MEXTRAM model
- [6] <http://hbt.ucsd.edu/>. UCSD HBT model. 2000. Rev 9.001a
- [7] <http://www.fbh-berlin.de/modeling.html>. FBH HBT model. 2005. ver 2.1
- [8] Ge Ji, Jin Zhi, Liu Xinyu, et al. A VBIC model with voltage-dependent carrier velocity and depletion-layer thickness. *Journal of Semiconductors*, 2008, 29(11): 171
- [9] Agilent ADS 2008 manual: user-defined models: 81-115
- [10] Tiwari S. A new effect at high currents in heterostructure bipolar transistors. *IEEE Electron Device Lett*, 1988, 9(3): 142
- [11] Kirk C T. A theory of transistor cutoff frequency (f_i) falloff at high current densities. *IRE Trans Electron Devices*, 1962, 9(2): 164
- [12] Ge Ji, Jin Zhi, Su Yongbo, et al. A physics-based charge-control model for InP DHBT including current-blocking effect. *Chin Phys Lett*, 2009, 26: 077302
- [13] Iwamoto M, Root D E, Scott J B, et al. Large-signal HBT model with improved collector transit time formulation for GaAs and InP technologies. *IEEE MTT-S Int Microwave Symp Dig*, 2003, 2: 635
- [14] Degachi L, Ghannouchi F M. Systematic and rigorous extraction method of HBT small-signal model parameters. *IEEE Trans Microw Theory Tech*, 2006, 54(2): 682
- [15] Bousnina S, Mandeville P, Kouki A B, et al. Direct parameter-extraction method for HBT small-signal model. *IEEE Trans Microw Theory Tech*, 2002, 50(2): 529